DE GRUYTER
OPEN

Journal of Research in Physics Vol. 38, No. 1, 23 - 32 (2014/15)

doi:10.1515/jrp-2015-0003

Analysis of luminescence of Eu^{3+} doped $Lu_2Ti_2O_7$ powders with Judd-Ofelt theory

Katarina Vuković, Sanja Ćulubrk, Milica Sekulić, and Miroslav D. Dramićanin*
Vinča Institute of Nuclear Sciences, University of Belgrade, PO Box 522, Belgrade, Serbia
Corresponding author email: dramican@vinca.rs

Received: *October 26, 2015*

Abstract

Eu^{3+} doped $Lu_2Ti_2O_7$ particles of 6 to 10 nm in diameter are prepared by Pechini-type polymerized complex route based on polyesterification between citric acid (CA) and ethylene glycol. X-ray diffraction measurements confirmed that Eu^{3+} doped $Lu_2Ti_2O_7$ powders crystallized in the face-centered cubic lattice (Fd3m). Emission spectra displayed characteristic $^5D_0 \rightarrow ^7 F_J$ ($J = 0, 1, 2, 3$ and 4) spin forbidden f-f electronic transitions of the Eu^{3+} ions with the most pronounced emission coming from $^5D_0 \rightarrow ^7 F_2$ and with the emission decays varying between 0.75 and 0.60 ms for samples doped with different concentration of Eu^{3+}. The Judd-Ofelt theory was applied to the experimental data for the quantitative determination of optical parameters such as Ω_2, Ω_4 Judd-Ofelt parameters, radiative and nonradiative transition rates and emission quantum efficiency. It was observed that, for all the samples, $\Omega_2 >> \Omega_4$. The luminescence quantum yields were calculated by means of the Judd-Ofelt theory and the highest value 60.83 % is obtained for particles doped with concentration of 3 % Eu^{3+}.

Key words: Judd-Ofelt analyses, Eu^{3+}, luminescence, lanthanides.

1. Introduction

In the last decades, much research has been focused on luminescent materials containing trivalent lanthanide ions, Ln^{3+} [1]. Rare earth compounds have been widely used in high performance luminescent devices, magnets, catalysts, and other functional materials. Materials containing RE ions as activators show a series of sharp absorption and emission lines from the infrared up to the ultraviolet region [2]. Pyrochlore compounds are inherent ionic conductors whose properties may be altered by changing the processing conditions and doping of different elements on various sites. These materials can also be used as solid electrolyte in solid oxide fuel cell [3]. Structurally, pyrochlore exhibits ?uorite type structure. The $Lu_2Ti_2O_7$ phase is known to have the cubic (Fd3m) pyrochlore structure

with a large unit cell constant of about 10 Å. [4-5]. Pyrochlore oxides have attracted much attention because, depending on the chemical elements involved, they display a large variety of physical and chemical properties and therefore, potential applications in many areas of technological interest [6]. In the present work, we propose a Pechini method to synthesize Eu^{3+} doped $Lu_2Ti_2O_7$ with a pyrochlore type structure. Also, we present structural, morphological and optical characterization of Eu^{3+} doped pure phase $Lu_2Ti_2O_7$ powders, and discuss obtained results. Photoluminescence measurements are performed to analyze emission and emission decay characteristics of powders. The Judd-Ofelt analysis of the emission spectra of Eu^{3+} ions was performed, which allowed to calculate radiative and non-radiative transition probabilities, Judd-Ofelt intensity parameters and the quantum efficiency of the Eu^{3+} emission in the $Lu_2Ti_2O_7$ particles. Therefore, the analysis provides the best concentration of Eu^{3+} ions that delivers $Lu_2Ti_2O_7$ particles with the best luminescence properties. So far no data on the radiative and non-radiative transition probabilities and quantum efficiencies of emission of RE impurities in $Lu_2Ti_2O_7$ particles have been reported.

2. Materials and methods

2.1. Synthesis of $Lu_2Ti_2O_7$:Eu^{3+} powder

A set of six samples were prepared with different Eu^{3+} concentrations (1; 3; 5; 7; 10 and 15 at.%) by Pechini-type polymerized complex route based on polyesterification between citric acid (CA) and ethylene glycol. In brief, for synthesis of rare earth doped $Lu_2Ti_2O_7$ particles, titanium (IV)-isopropoxide, lutetium (III)-nitrate, citric acid and ethylene glycol were mixed in 1:1:5:20 molar ratio. In the first step, titanium (IV)-isopropoxide (Alfa Aesar, 97 %) was dissolved in ethylene glycol (Lach-Ner, 99 %). Then citric acid (Kemika, 99.5 %) was added to the solutions. Appropriate amounts of Lu_2O_3 (Alfa Aesar, 99.9 %) and Eu_2O_3 (Alfa Aesar, 99.9 %) were dissolved in hot, concentrated nitric acid, evaporated to dryness and joined with titanium (IV)-isopropoxide/EG/CA mixture. The mixtures were stirred for 1h at 60°C until they became transparent and further heated at 130°C for few hours to promote polymerization and transform to resin like form. Black, amorphous resins were fired at 350°C for 30 minutes and grounded to a powder. In order to obtain pure phase $Lu_2Ti_2O_7$ the particles were calcined at 820°C for 4 hours.

2.2. Instruments and measurements

X-ray diffraction (XRD) measurements were performed using Rigaku SmartLab diffractometer. Diffraction data were recorded in a 2θ range from 10° to 90°, counting 0.7°/minute in 0.02° steps. Relevant results of structural analysis (unit cell parameter, crystal coherence size, microstrain values and data fit parameters) were obtained using built-in package software. Microstructural characterization was done using a JEOL JSM-6610LV scanning electron microscope (SEM). An acceleration voltage of 20 kV was used for the analyses. Photoluminescence (PL) measurements were done on Fluorolog-3 Model FL3-221 spectroflurometer system (Horiba Jobin-Yvon), utilizing 450 W Xenon lamp as the excitation source for emission measurements and Xenon-Mercury pulsed lamp for lifetime measurements. TBX-04-D PMT detector is used for lifetime and steady state acquisitions.

3. Results and discussion

3.1. XRD analysis

$Lu_2Ti_2O_7$ crystallizes in the face centered cubic structure, space group Fd3m, No. 227, which was confirmed by XRD analyses after calcination at 820°C for 4h. XRD patterns of Eu^{3+} doped $Lu_2Ti_2O_7$ are presented in Fig. 1. The main diffraction peaks are indexed according to the ICDD card No. 01-074-9562 [7].

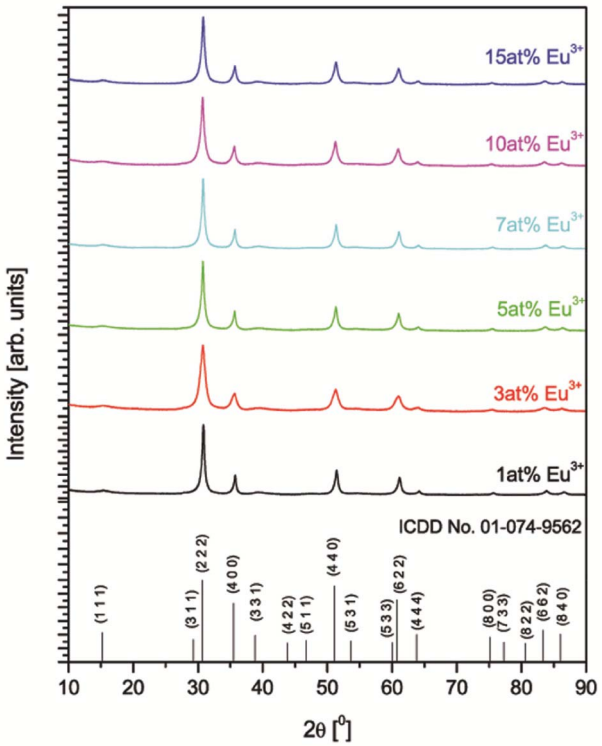

Figure 1. XRD patterns of Eu^{3+} doped $Lu_2Ti_2O_7$ powder samples.

Relevant results of structural analysis (unit cell parameter, crystal coherence size and microstrain values) are presented in Table 1. Microstrain values are low suggesting good ion ordering in the crystals.

Table 1. Structural parameters obtained from XRD measurements.

$Lu_2Ti_2O_7$	Crystallite size (nm)	a (Å)	Microstrain (%)	Rwp (%)	Rp (%)	GOF
1 at.% Eu^{3+}	9.7(12)	10.0631(5)	0.44(12)	5.08	3.43	2.5240
3 at.% Eu^{3+}	6.2(6)	10.0874(11)	0.38(3)	5.17	3.69	2.6836
5 at.% Eu^{3+}	8.5(9)	10.0775(13)	0.52(11)	5.29	3.54	2.6466
7 at.% Eu^{3+}	8.9(10)	10.0779(6)	0.48(12)	5.20	3.60	2.6328
10 at.% Eu^{3+}	7.3(5)	10.0862(8)	0.49(9)	4.85	3.39	2.4379
15 at.% Eu^{3+}	7.9(8)	10.0877(8)	0.48(14)	4.50	3.24	2.2744

3.2. SEM analysis

Morphology of the representative sample $Lu_2Ti_2O_7$:1 at.% Eu^{3+} obtained through Pechini-type polymerized complex route is shown in Fig. 2. The micrograph provided by SEM analysis, indicated that $Lu_2Ti_2O_7$:1 at.% Eu^{3+} consists of large chunks, up to several microns in size, formed wholly of smaller particles.

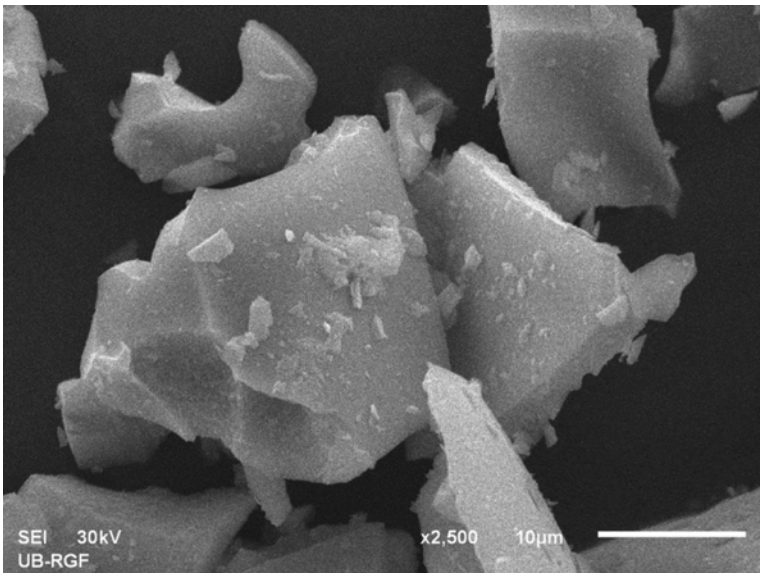

Figure 2. SEM image taken from $Lu_2Ti_2O_7$:1 at.% Eu^{3+} powder.

3.3. Photoluminescence emission spectra and lifetime measurements

Emission spectra of $Lu_2Ti_2O_7$ samples doped with 1 at.%, 3 at.%, 5 at.%, 7 at.%, 10 at.%,15 at.% of Eu are measured, and the representative spectrum is presented in Fig 3. Due to the even number of electrons in the 4f shell ($4f^6$ configuration), the crystal-field perturbation by the crystalline host matrix lifts partly or completely the degeneracies of the Eu^{3+} levels [8]. Therefore, emission spectra show five characteristic bands centered around 17287, 16896, 16217, 15333 and 14257 cm^{-1} that origin from $^5D_0 \rightarrow ^7F_i$ ($i = 0, 1, 2, 3$ and 4) spin forbidden f-f electronic transitions of the Eu^{3+} ions. The $^5D_0 \rightarrow ^7F_1$ transition is magnetic dipole in nature and follows the selection rule $\Delta J = 1$. Its intensity is independent of the host matrix. On the other hand, the $^5D_0 \rightarrow ^7F_i$ ($i = 2, 4, 6$) are "the forced" electric dipole transitions, known to be forbidden by the Laporte selection rule, and may occur due to the mixing of the 4f orbitals with opposite parity at the low symmetry sites. The $^5D_0 \rightarrow ^7F_2$ is known as a hypersensitive transition because it is easily affected by the local environment around the europium ion, and its intensity depends on the symmetry of the crystal field around the europium ion. The intensity of $^5D_0 \rightarrow ^7F_2$ transition is the most intense across the emission spectra. The $^5D_0 \rightarrow ^7F_0$ transition is not allowed since $0 - 0$ transitions are forbidden by the selection rule $J = 0 \rightarrow J' = 0$. The appearance of this transition is mainly due to the J-mixing effect [9] and indicates that the Eu^{3+} ion is located in a site without an inversion center. Low energy transitions, $^5D_0 \rightarrow ^7F_3$ and $^5D_0 \rightarrow ^7F_4$, are also clearly visible. Emissions from $^5D_0 \rightarrow ^7F_5$ (12990-13510 cm^{-1}) and $^5D_0 \rightarrow ^7F_5$ (11900-12350 cm^{-1}) transitions could not be detected due to the instrument limitations.

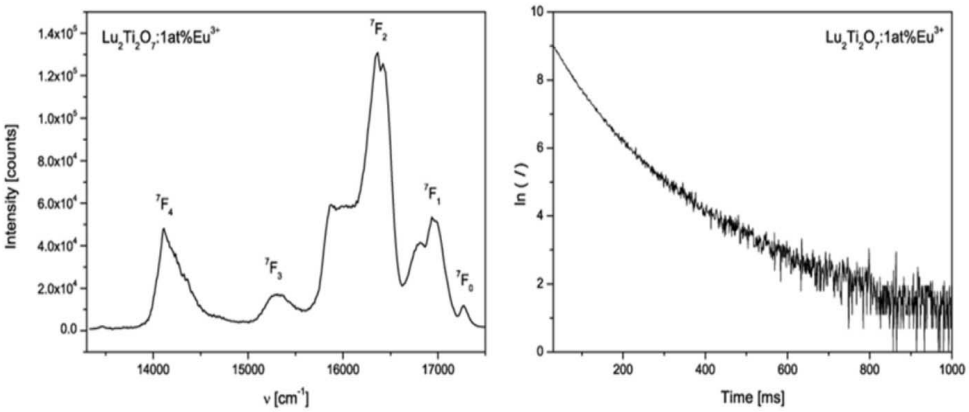

Figure 3. Representative emission spectrum (left) and emission decay (right) of $Lu_2Ti_2O_7$:Eu^{3+} powder.

The emission decays of the $^5D_0$ emitting level of $Lu_2Ti_2O_7$:Eu^{3+} powder are obtained under 394 nm excitation. Average lifetime values are calculated using the following equation:

$$\tau_{\text{avg}} = \frac{\int_0^\infty tI(t)dt}{\int_0^\infty I(t)dt} \tag{1}$$

where $I(t)$ represents the luminescence intensity at time t, corrected for the background. The results of the calculations are presented in Table 2.

Table 2. Lifetimes of the $^5D_0$ emission level of Eu^{3+} in $Lu_2Ti_2O_7$ particles doped with different concentration of Eu^{3+}.

Eu^{3+} doped $Lu_2Ti_2O_7$	
Eu^{3+} concentration (at. %)	Lifetime constant (ms)
1	0.70
3	0.74
5	0.71
7	0.75
10	0.66
15	0.60

In all samples the highest integral emission intensity is observed for the $^5D_0 \rightarrow ^7F_2$ transition. The intensity of this transition is shown in Figure 3, and the lifetime values in Table 2. The lifetime values of the $^5D_0$ level are similar up to 7 at. % Eu^{3+} ($\approx 0.70 - 0.75$ ms), but they experience a decrease at 10 at.% Eu^{3+} (≈ 0.66 ms).

3.4. Judd-Ofelt calculations and results

The Judd-Ofelt theory [10,11] describes intensities of transitions of lanthanides and actinides in solids and solutions, whereas the Judd-Ofelt parameters characterize the local structure and bonding in the vicinity of rare earth ions. This theory provides information

about oscillator strengths, radiative lifetime (τ_{R}) and transition probability (A). The analysis also provides values of quantum efficiency and estimates of the degree of Eu ligand covalency. According to J-O theory [10,11] the theoretical expression for oscillator strength for an induced electric dipole transition from the ground state to an excited state is:

$$f = \frac{8\pi^2 mc\nu}{3h(2J+1)} \frac{(n^2+2)^2}{9n} \sum_{\lambda=2,4,6} \Omega_\lambda (\Psi J \| U^\lambda \| \Psi' J')^2 \tag{2}$$

where h denotes the Planck constant (6.63×10^{-27} erg·s), $2J+1$ is the degeneracy of the initial state, n is the refractive index, Ω_λ are the Judd-Ofelt parameters and $\|U^\lambda\|$ the double reduced matrix elements of unit tensor operators whose values are independent of the local environment of the ion. According to the Judd-Ofelt theory the spontaneous transition probability, A, is related to its dipole strength according to the following equation:

$$A(\Psi' J'; \Psi J) = \frac{64\pi^4 e^2}{3h(2J+1)\lambda^3} \left[n \left(\frac{n^2+2}{9} \right)^2 D_{\mathrm{ED}} + n^2 D_{\mathrm{MD}} \right] \tag{3}$$

where D_{ED} and D_{MD} are the electric and magnetic dipole strengths (in esu^2 cm^2), respectively. Transition probabilities of the rare earths are composed mainly of the electric dipole contribution $^5\mathrm{D}_0 \rightarrow^7 \mathrm{F}_\mathrm{i}$ ($i = 2, 4$) and to a much lesser extent by the magnetic-dipole contribution $^5\mathrm{D}_0 \rightarrow^7 \mathrm{F}_1$. The $^5\mathrm{D}_0 \rightarrow^7 \mathrm{F}_3$ transition is forbidden according to Judd-Ofelt theory both in magnetic and induced electric dipole scheme, and this transition can only gain intensity via J-mixing [12,13]. Also, the $^5\mathrm{D}_0 \rightarrow^7 \mathrm{F}_0$ transition is strictly forbidden according to the standard Judd-Ofelt theory. Due to the above mentioned, these two transitions will not be considered in the determination of transition probabilities. The intensity of $^5\mathrm{D}_0 \rightarrow^7 \mathrm{F}_1$ magnetic dipole transition is largely independent of the environment and can be considered in a first approximation to be constant [14]. The magnetic dipole transition can be calculated by theory [12,15] as:

$$D_{\mathrm{MD}} = 9.6 \times 10^{-42} \mathrm{esu}^2\,\mathrm{cm}^2. \tag{4}$$

The strength of all induced electric dipole transitions is:

$$D_{\mathrm{ED}}(J, J') = e^2 \sum_{\lambda=2,4,6} \Omega_\lambda |\langle \Psi J \| U^\lambda \| \Psi J' \rangle|^2 \tag{5}$$

where $|\langle \Psi J \| U^\lambda \| \Psi J' \rangle|^2$ are squared reduced matrix elements whose values are independent of the host matrix. For the case of Eu^{3+} these values are given in Ref. [15-17]. In the case of Eu^{3+} emission, Judd-Ofelt intensity parameters can be evaluated solely from the emission spectrum because non-diagonal elements of the $|\langle \Psi J || U^\lambda || \Psi J' \rangle|^2$ matrix have zero values:

$$\Omega_\lambda = \frac{D_{\mathrm{MD}} \nu_1^3}{e^2 \nu_\lambda^3} \frac{9n^3}{n(n^2+2)^2 |\langle \Psi J \| U^\alpha \| \Psi J' \rangle|^2 \frac{\int I_\lambda(\nu_\lambda)}{\int I_1(\nu_1)}} \tag{6}$$

For the J-O calculations the value of refraction index of 2.12 is taken from the literature [18]. Then, it is possible to calculate the ratio of the radiative transition probabilities A

of different transitions from the ratios of areas S under the corresponding emission bands [17,19]:

$$A(^5\mathrm{D}_0 \rightarrow ^7\mathrm{F}_{2,4}) = \mathrm{A}(^5\mathrm{D}_0 \rightarrow ^7\mathrm{F}_1) \times \frac{\mathrm{S}(^5\mathrm{D}_0 \rightarrow ^7\mathrm{F}_{2,4})}{\mathrm{S}(^5\mathrm{D}_0 \rightarrow ^7\mathrm{F}_1)} \tag{7}$$

The total radiative rate, A_{R}, defined as the sum of all radiative rates, can be further used to evaluate the non radiative rate, A_{NR}, the value of luminescence intensity ratio R and the emission quantum efficiency, η (ratio between number of photons emitted by the Eu^{3+} ion to those absorbed by the Eu^{3+} ion).

The Ω_2 intensity parameter depends on the symmetry of the local surrounding around the Eu^{3+} site and is strongly affected by the degree of the covalence bond between Eu^{3+} and ligands. Ω_4 and Ω_6 parameters are associated to the viscosity and rigidity of the host material. The stronger the covalence the higher the value of Ω_2 [20,21]. Luminescence intensity ratio $R = \frac{^5\mathrm{D}_0 \rightarrow ^7\mathrm{F}_2}{^5\mathrm{D}_0 \rightarrow ^7\mathrm{F}_1}$, also known as asymmetry ratio [22], represents the measure of degree of Eu-O covalency [23]. As the value of R increases, the symmetry around the trivalent europium reduces [24]. Ω_2 and R reveal complementary physical information on the bonding nature between the Eu^{3+} ion and the surrounding anions. Furthermore, the R value depends on the J-O parameter Ω_2 which is used to explain the short range effects in the local structure around the Eu^{3+} ions and Eu-O covalence [25]. The Ω_6 intensity parameter could not be determined because the $^5\mathrm{D}_0 \rightarrow ^7\mathrm{F}_6$ emission in this sample couldn't be detected due to the instrumental limitations.

Calculated Judd-Ofelt parameters show variations with different concentrations of Eu^{3+}, and their values are presented in Table 3.

Table 3. Intensity parameters, radiative and non-radiative transition rates, quantum efficiencies and asymmetry ratios of Eu^{3+} emission from $Lu_2Ti_2O_7$ particles prepared with different concentration of Eu^{3+}.

n (%)	Ω_2 (10^{-20} cm^{-1})	Ω_4 (10^{-20} cm^{-1})	A (s^{-1})	A_{NR} (s^{-1})	η (%)	R
1	4.68	2.53	717.30	711.27	50.2	3.23
3	5.52	3.02	822.15	529.22	60.8	3.91
5	5.02	2.58	752.51	655.94	53.4	3.56
7	4.83	2.46	728.60	604.77	54.6	3.43
10	5.25	2.62	777.34	737.80	51.3	3.72
15	4.97	2.48	743.17	923.51	44.6	3.53

Calculated values of the Ω_2 and Ω_4 parameter are similar for all Eu^{3+} concentrations. This trend is displayed in Figure 4(a). The $\Omega_2 > \Omega_4$ trend confirms the existence of covalence between the Eu^{3+} ion and ligands as well as the asymmetry around the metal ion site [26]. The obtained results for Ω_2 and Ω_4 are similar and no significant changes are observed. Likewise, calculated values of asymmetric ratio R are also close. The asymmetric ratio R in dependence of different atomic percentage of Eu^{3+} (1, 3, 5, 7, 10 and 15 %) is presented in Figure 4(b). These results indicates that the local environment of the ion was stable and does not change with concentrations in this range [27].

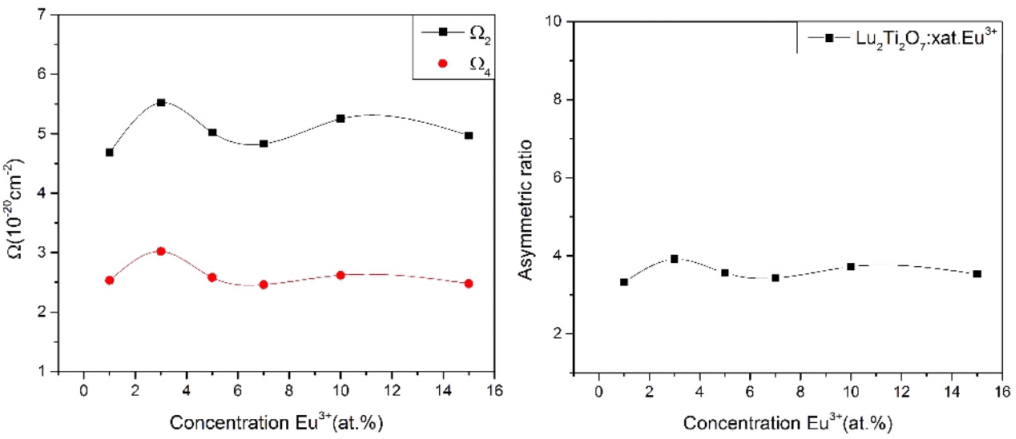

Figure 4. (a) Ω_2 (black squares) and Ω_4 (red circles) intensity parameters, and (b) asymmetric ratio as a function of Eu^{3+} (1, 2, 4, 8 and 12 %) concentration.

Figure 5(a) shows changes of the radiative and non-radiative transition rates of Eu^{3+} emissions in samples doped with different concentration of Eu^{3+}. The results for quantum efficiency are displayed in Figure 5(b). The highest value of the quantum efficiency is obtained for concentration of 3 % and it is 60.83 %, and the lowest value is obtained for the 15 % and it is 44.58 %. The decrease of the quantum efficiency with the increase of the dopant concentration above 10 % is the consequence of high cross-relaxation processes.

It is acknowledged that Judd-Ofelt theory estimates transition probabilities with accuracy generally not worse than 10 % [28].

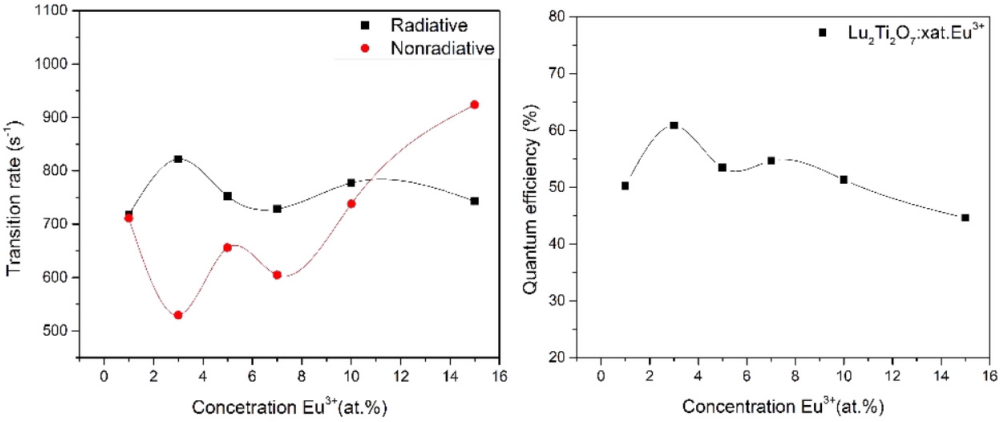

Figure 5. (a) Radiative transition rate (black squares) and non-radiative transition rate (red circles), and (b) quantum efficiency as a function of Eu^{3+} (1, 2, 4, 8 and 12 %) concentration.

4. Conclusion

To conclude, a set of samples with different Eu^{3+} concentrations (1; 3; 5; 7; 10 and 15 at. %) doped $Lu_2Ti_2O_7$ particles has been prepared with Pechini-type polymerized com-

plex route. Particles doped with 3 % of Eu^{3+}, exhibiting quantum efficiency of emission of 60.9 %, showed the best luminescence properties. In all samples the Judd-Ofelt intensity parameter Ω_2 was larger than Ω_4 parameter showing existence of covalence between the Eu^{3+} ion and ligands as well as the asymmetry around the metal ion sites.

Acknowledgments

Authors acknowledge the financial support of the Ministry of Education and Science of the Republic of Serbia (Project no. 45020).

References

[1] T. Justel, H. Nikol and C. Ronda, Angew. Chem. Int. Ed. **37**, 3084 (1998).

[2] A. J. Kenyonn, C. E. Chryssou and C. W. Pitt, J. Appl. Phys. **91**, 367 (2002).

[3] S. A. Kramer, H. L. Tuller, Solid State Ion. **82**, 15 (1995).

[4] E. Aleshin and R. Roy, J. Am. Ceram. Sot. **45**, 18 (1962).

[5] D. D. Hogarth, Am. Mineral. **62**, 403 (1977).

[6] M. Subramanian, G. Aravamudan, G. V. Subba Rao, Prog. Solid State Chem. **15**, 55 (1983).

[7] A. V. Shlyakhtina, A. V. Knotko, M. V. Boguslavskii, S. Yu. Stefanovich, D. V. Peryshkov, I. V. Kolbanev, L. G. Shcherbakova, Solid State Ion. **176**, 2297 (2005).

[8] K. Binnemans, Coord. Chem. Rev. **295**, 1 (2015).

[9] P. A. Tanner, Y. Y. Yeung, and L. Ning, J. Phys. Chem. A **117**, 2771 (2013).

[10] B. R. Judd, Phys. Rev. **127**, 750 (1962).

[11] G. S. Ofelt, J. Chem. Phys. **37**, 511 (1962).

[12] M. J. Weber, T. E. Varitimos, and B. H. Matsinger, Phys. Rev. B **8**, 47 (1973).

[13] J. E. Lowther, J. Phys. C **7**, 4393 (1974).

[14] C. Görller-Walrand, L. Fluyt, A. Ceulemans, and W.T. Carnall, J. Chem. Phys. **95** (1991).

[15] M. H. V. Werts, R. T. F. Jukes, and J. W. Verhoeven, Phys. Chem. Chem. Phys. **4**, 1542 (2002).

[16] W. T. Carnall, P. R. Fields, and K. Rajnak, J. Chem. Phys. **49**, 4412 (1968).

[17] L. Đacanin, S. R. Lukić, D. M. Petrović, M. Nikolić, and M. D. Dramićanin, Physica B **406**, 2319 (2011).

[18] D. D. Gulamova, Geliotekhnika 2009(1), P55-66 CAPLUS.

[19] D. Uma Maheswari, J. Suresh Kumar, L. R. Moorthy, K. Jang, and M. Jayasimhadri, Physica B **403**, 1690 (2008).

[20] C. Koeppen, S. Yamada, G. Jiang, A. F. Garito, and L. R. Dalton, J. Opt. Soc. Am. B: Opt. Phys. **14**, 155 (1997).

[21] S. S. Braga, R. A. Sá Ferreira, I. S. Gonçalves, M. Pillinger, J. Rocha, J. J. C. Teixeira-Dias, and L. D. Carlos, J. Phys. Chem. B **106**, 11430 (2002).

[22] A. Patra, E. Sominska, S. Ramesh, Y. Koltypin, Z. Zhong, H. Minti, R. Reisfeld, and A. Gedanken, J. Phys. Chem. B **103**, 3361 (1999).

[23] G. Ehrhart, M. Bouazaoui, B. Capoen, V. Ferreiro, R. Mahiou, O. Robbe, and S. Turrell, Opt. Mater. **29**, 1723 (2007).

[24] K. Binnemans, K. Van Herck, and C. Görller-Walrand, Chem. Phys. Lett. **266**, 297 (1997).

[25] P. Babu, and C. K. Jayasankar, Physica B **279**, 262 (2000).

[26] M. Kumar, T. K. Seshagiri, and S. V. Godbole, Physica B **410**, 141 (2013).

[27] G. Zhou, Z. Wang, B. Zhou, Y. Zhao, G. Zhang, S. Wang, Opt. Mater. **35**, 774 (2013).

[28] R. Rolli, K. Gatterer, M. Wachtler, M. Bettinelli, A. Speghini, D. Ajó, Spectrochim. Acta Mol. Biomol. Spectrosc. **57**, 2009 (2001).